Fiber Fabry–Perot Interferometer with Mode-Converting Bragg Gratings

Dietmar Johlen, Peter Klose, Hagen Renner, and Ernst Brinkmeyer

***Abstract*—Bragg gratings are genuine narrow band reflectors. However, for several applications narrow band transmission filters are of interest. It is demonstrated that a pair of mode-converting Bragg gratings in a Fabry–Perot interferometer configuration yields a nonreflecting, narrow-band transmission filter. A more detailed investigation shows further a different mode of operation where narrow band reflection occurs in resonance. It is shown experimentally how both modes of operation are attained by UV trimming of the Fabry–Perot interferometer. A mathematical model for the mode-converting Fabry–Perot interferometer is given.**

***Index Terms*—Bragg gratings, mode conversion, output coupler, transmission filter, two-mode fiber.**

I. Introduction

BRAGG gratings are known as narrow-band reflectors and are employed in numerous applications. For several applications it is desirable to have narrow band spectral response as in Bragg gratings but without reflection. In this paper we demonstrate that mode-converting gratings are attractive for optical filter design. Tilted Bragg gratings have been demonstrated as intermodal converters in two-mode fiber [1] and two-mode integrated optical waveguides [2]. However, waveguides of interest such as standard communication fibers are single-moded in general. Such fibers cannot host mode-converting Bragg gratings, whereas splicing two-mode fiber sections into a single-mode fiber seems to be intricate. Our solution makes use of the high ultraviolet (UV)-induced index increase available in hydrogen loaded fibers of about $\Delta n_{\mathrm{UV}} \approx 10^{-2}$ [3]. This enables direct UV writing of two-mode sections into an elsewhere single-mode fiber. A tilted Bragg grating written afterwards in that section couples the fundamental LP_{01}-mode and the first higher-order LP_{11}-mode. The adjacent single-mode fiber regions act as highly selective mode filters and the converted light experiences high losses outside the two-mode section [4].

In particular, this concept is used here to realize narrow-band transmission filters which—unlike ordinary Fabry–Perot interferometers—do not reflect the incident light at either side of the transmission peak.

But this is not the only mode of operation of the mode-converting Fabry–Perot interferometer. We further show that a mode-converting Fabry–Perot interferometer can exhibit simultaneous narrow-band transmission and reflection in resonance. This unique property is demonstrated as a narrow-band output-coupler for fiber lasers.

Manuscript received February 1, 2000; revised June 5, 2000.

The authors are with the Technische Universität Hamburg-Harburg, Optik und Messtechnik, Eißendorfer Straße 40, D-21073 Hamburg, Germany (e-mail: dietmar.johlen@icn.siemens.de).

Publisher Item Identifier S 0733-8724(00)09105-2.

In order to understand the underlying processes for these rather different modes of operation a mode-converting Fabry–Perot interferometer can exhibit, we are presenting a theoretical model. The conditions for either mode of operation are derived from the model and discussed.

It is shown experimentally how both modes of operation can be achieved in a well defined way by UV trimming the Fabry–Perot interferometer after fabrication.

Regarding the high reflectivity of the Bragg gratings this approach has the potential to operate a fiber laser equipped with this novel narrow-band filter on a single longitudinal mode. The technique of UV writing of two-mode fiber sections can also be applied to photosensitive integrated optical waveguides.

II. Experimental Setup

Starting point is a truly single-mode, photosensitive fiber (CD 120.02, OFTC, Sydney). A predetermined typically 10 mm long section of the hydrogen-loaded fiber (3 mol%) is homogeneously irradiated with a specified fluence of UV-light at $\lambda = 244$ nm by means of an Argon-Ion Laser [4].

In this way, the refractive index of the fiber core is increased up to a level where this fiber section becomes two-moded while all the rest of the fiber remains single-mode. The pre-irradiation for creating the two-mode section is carried out by scanning the focused UV-beam along the fiber at a power of about $P_{\mathrm{UV}} = 80$ mW and writing speed of $v_{\mathrm{UV}} = 2.5$ mm/min. The UV beam is focused to a spot diameter of 200 μm for a better writing efficiency. The dependence of the UV-induced index increase on the fluence is important for a well defined writing of two-mode sections in a photosensitive single-mode fiber. It has been analyzed by a Fabry–Perot interferometer [3] by monitoring the consecutive resonances while the section in between the grating pair is homogeneously illuminated. An index increase of about 4×10^{-3} is necessary for two-mode wave guiding in the OFTC fiber. In the next step, a phase mask (period on the mask $\Lambda = 1069$ nm) is placed on top of the fiber at an angle α' as to yield a blaze angle $\alpha = 3^{\circ}$ for the grating fringes inside the core. For this angle maximum mode-conversion is achieved. The two tilted Bragg gratings which are to serve as mode-converters are written one after the other in a scanning mode at either end of the two-mode section as schematically shown in Fig. 1.

III. Narrow-Band Transmission Filter Without Reflection

The principle of operation of the transmission filter is shown in Fig. 1. A pair of mode-converting Bragg gratings written into a two-mode section forms a mode-converting Fabry–Perot

0733–8724/00$10.00 © 2000 IEEE

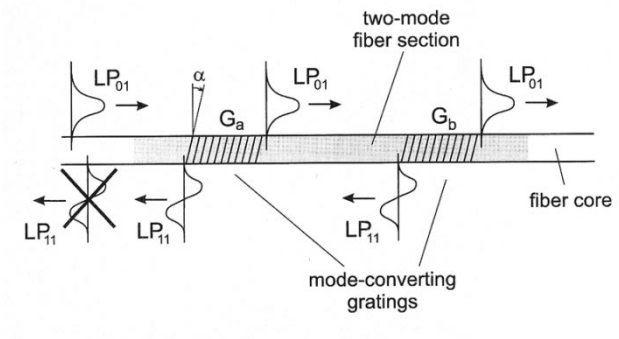

Fig. 1. Setup of two mode-converting Bragg gratings in a two-moded section of an elsewhere single-mode fiber.

interferometer [5]. In a particular wavelength range given by the effective indexes within the gratings in the two-mode section, mode coupling occurs between the fundamental LP_{01} and higher order LP_{11} mode. If the tilt angle is properly chosen (see Fig. 5) the conversion is highly efficient. In the forward direction the power is propagated only by the fundamental LP_{01} mode, while in the backward direction the power is carried only by the first higher-order LP_{11} mode. In this wavelength range incident light travelling in $+z$-direction in the fundamental mode will be nearly completely converted by the grating into the LP_{11} mode. Vice versa, light travelling in the LP_{11} mode in $-z$-direction is reconverted to the LP_{01} mode. Therefore, starting with an input wave in $+z$-direction, all the forward traveling light tends to be in the LP_{01}-mode and all the backward travelling light is essentially in the LP_{11}-mode. In this way, a resonator is formed which behaves like a two-mirror Fabry–Perot interferometer. In particular, at resonance the light is transmitted in the fundamental mode while out of resonance all the light is reflected into the first-higher order mode and lost by radiation outside the two-mode section, thus forming a narrow band transmission filter without reflection [5]. This unique property can neither be attained in single-mode fiber because there is no mode-conversion nor in two-mode fiber because there is no suppression of the reflected light. The experimental realization of the mode-converting Fabry–Perot interferometer consists of two 2-mm-long tilted gratings separated by 6 mm. The normalized transmission spectrum of the Fabry–Perot filter described above is measured with a grating spectrometer and shown in Fig. 2. The two prominent transmission minima at different wavelengths in Fig. 2 correspond to LP_{01}-LP_{01} reflection and LP_{01}-LP_{11} conversion. Note, that the Fabry–Perot resonances are far too narrow to be resolved by the grating spectrometer. Therefore, the spectrum in Fig. 2 is similar to that one of a corresponding one-grating structure [4]. The wavelength range of interest here is the LP_{01}-LP_{11} conversion band located around $\lambda_{11} = 1552$ nm. Using a tunable laser diode in a piezocontrolled continuous scanning mode the Fabry–Perot resonances can be detected both in transmission and reflection as shown schematically in Fig. 3. The transmission near a resonance is shown in Fig. 4. Its fullwidth at half-maximum (FWHM) width is 6.6 pm. Since the continuous scanning range is limited to about 30 pm the neighbor resonances cannot be measured in a single scan but can be determined by using the coarse scanning mode. The result is a free spectral range FSR $= 120$ pm and thus a finesse of $\mathcal{F} = 18$.

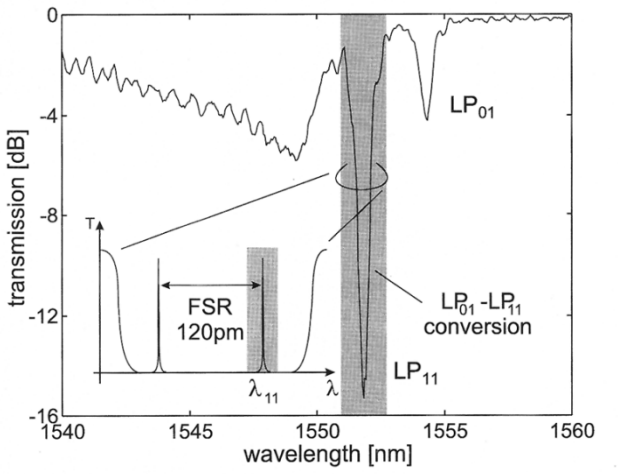

Fig. 2. Transmission spectrum of a Fabry–Perot interferometer with mode-converting Bragg gratings. The shaded wavelength interval denotes the range of the mode-conversion. The inset illustrates the Fabry–Perot resonances within the mode-conversion stop-band that are not resolved by the optical spectrum analyzer.

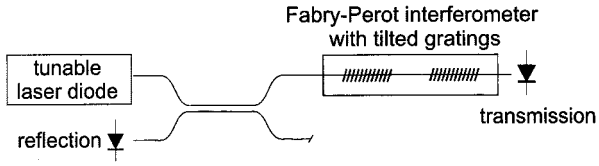

Fig. 3. Setup for analyzing the Fabry–Perot resonances with a tunable laser source. The laser can be fine tuned by about 30 pm.

Due to resonator losses which have to be considered for further work with these Fabry–Perot filters [6], [7] the maximum transmittance is $T_{\max} = 52\%$ at present. The minimum transmission is more than 12 dB below its maximum and, most important, the return loss is higher than 20 dB. As a potential application the mode-converting Fabry–Perot interferometer can be used as a filter element for a linear fiber laser with the potential of operation on one longitudinal mode.

IV. A More Detailed Investigation of the Mode-Converting Fabry–Perot Interferometer

A tilted grating in a two-mode fiber section is not only a mode-converter (LP_{01}-LP_{11}). It can also mediate a coupling between the fundamental mode (LP_{01}-LP_{01}) and the first higher order mode (LP_{11}-LP_{11}) with itself, respectively. The strength of this coupling is expressed by the coupling coefficients C_{kl}^{1} and depends on the tilt angle α of the grating. The coupling factors are calculated from the overlap integral of the involved modes

$$C_{kl}^{1}(\alpha) = \frac{\int \mathcal{E}_k^*(x,y)\epsilon_1(x,y,\alpha)\mathcal{E}_l(x,y)\,dx\,dy}{\int \mathcal{E}_0^*(x,y)\epsilon_1(x,y,\alpha=0)\mathcal{E}_0(x,y)\,dx\,dy} \qquad (1)$$

where $\mathcal{E}_k$ and $\mathcal{E}_l$ denote the modes of the electric field and ϵ_1 stands for the Fourier component of the electric permeability with the periodicity $\Lambda/(2\cos\alpha)$ of the tilted grating. The index

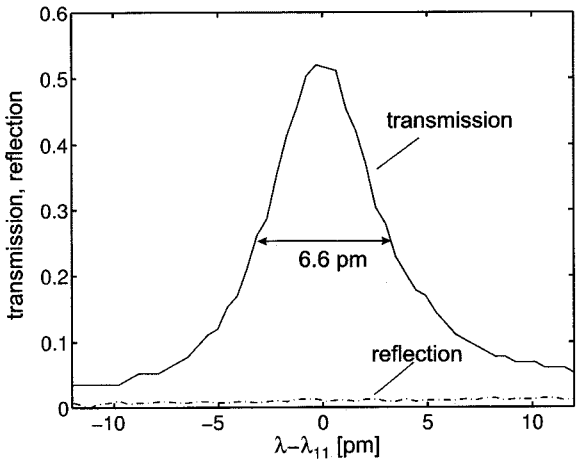

Fig. 4. Scan of the Fabry–Perot resonance around $\lambda_{11} = 1552$ nm. Within the stop-band of the fiber Bragg grating the resonances have a FWHM width of 6.6 pm and a free spectral range of 120 pm.

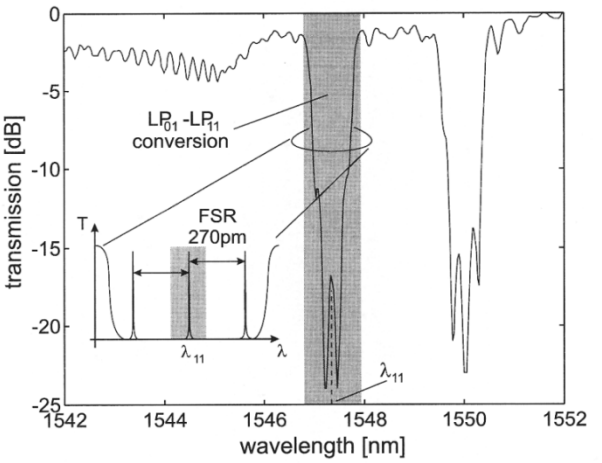

Fig. 6. Occurrence of mode reflection and mode conversion within the Fabry–Perot resonator.

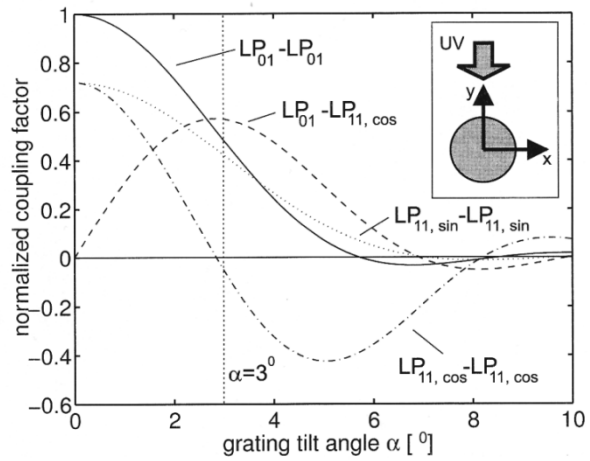

Fig. 5. Coupling factor between the modes versus the tilt angle α of the grating. The grating is tilted about the axes y.

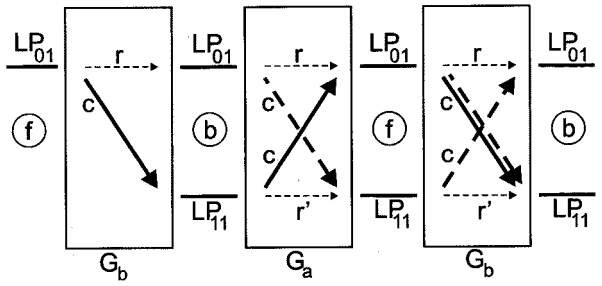

Fig. 7. Transmission spectrum of the Fabry–Perot interferometer with reflection in resonance. The two minima are caused by LP_{01} reflection into the LP_{01}-mode and conversion into the LP_{11}-mode. The Fabry–Perot resonances are not fully resolved by the spectrum analyzer (resolution 0.2 nm). The inset indicates the Fabry–Perot resonances within the mode-conversion stop-band.

"0" denotes the fundamental mode. The coupling coefficients of interest are shown in Fig. 5 as a function of the grating tilt angle.

Throughout the text LP_{11}-mode is understood as the $LP_{11,\cos}$-mode (see Fig. 5) in contrast to the orthogonal $LP_{11,\sin}$-mode. For completeness also the coupling coefficient for the $LP_{11,\sin}$-$LP_{11,\sin}$ coupling is shown in Fig. 5. This mode can be excited by the asymmetry of the index along axis y (see Fig. 5) due to the side writing of the grating [8].

The gratings presented in this paper have been written with a tilt angle of the grating fringes in the fiber core $\alpha \approx 3°$ where the mode-conversion (LP_{01}-LP_{11}) coupling coefficient has a maximum. For this tilt angle (see Fig. 5) the LP_{01}-LP_{01} coupling coefficient is of the same size as the mode-conversion coupling coefficient. Accordingly, the transmission spectra of mode-converting Fabry–Perot interferometers (see Figs. 2 and 6) show in addition to the stop-band for mode-conversion also a stop-band for fundamental-mode reflection (LP_{01}-LP_{01}). In addition to the dominant mode-conversion this leads to a small but not negligible out-of-band reflection of the fundamental mode in the stop-band of mode-conversion.

Fig. 7 shows the unfolded forward, f, and backward, b, light propagation in between the tilted gratings G_a and G_b. In the ideal case of pure mode-conversion, c, between the LP_{01}- and LP_{11}-mode only the solid bold lines in Fig. 7 are relevant. In this regime all the transmitted light propagates in the fundamental mode and all the reflected light propagates in the LP_{11}-mode and no reflection occurs since the Fabry–Perot interferometer is hosted by a single-mode fiber. Now, with out-of-band reflection possible due to a nonzero coupling factor for the LP_{01}-LP_{01} mode reflection, r, additional "transitions" occur in Fig. 7. In addition to the ideal case, the fundamental mode occurs in reflection and the higher order mode in transmission indicated by the dashed arrows in Fig. 7. Again, only the fundamental mode can be detected because a single-mode fiber hosts the Fabry–Perot interferometer.

This is comparable to coupled resonators. Here, the relation of the propagation constants β_{01} and β_{11} governs the behavior of the Fabry–Perot interferometer. Only if both resonators are

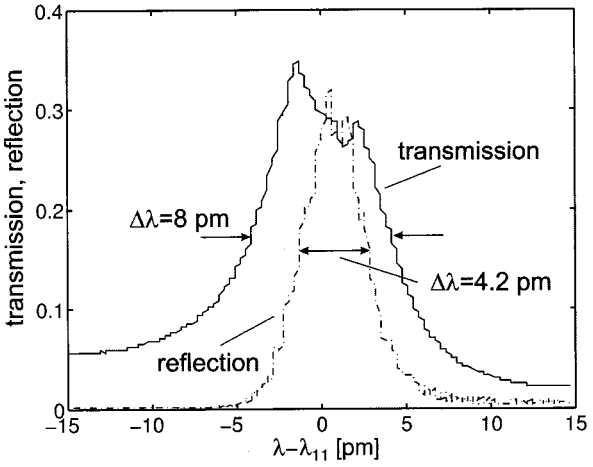

Fig. 8. High resolution scan of one Fabry–Perot resonance both in transmission and reflection.

in resonance at the same time, enough power can be transfered into the fundamental mode and a reflection can be detected.

In the following sections, this will be analyzed experimentally. We will further show how the Fabry–Perot interferometer can be tuned from one regime "no reflection in resonance" to the other "reflection in resonance" by UV illumination of the section between the gratings.

V. Reflection in Resonance

For this experiment the mode-converting Fabry–Perot interferometer is setup by two 2-mm-long tilted gratings (tilt angle $\alpha = 3°$) separated by 2 mm. The transmission spectrum of this Fabry–Perot interferometer is shown in Fig. 6.

One of the three resonances within the LP_{01}-LP_{11} mode-conversion stop-band at $\lambda_{11} = 1547.6$ nm has been analyzed in more detail with a tunable diode laser as described earlier (see Fig. 3). The normalized transmitted and reflected power is shown in Fig. 8. In contrast to the nonreflecting transmission filter a narrow-band reflection occurs in resonance of the Fabry–Perot interferometer [9]. A FWHM of 8 pm is achieved for the resonance in transmission and 4.2 pm for the resonance in reflection. The resonance in reflection is narrower than the resonance in transmission by a factor 2. This indicates the presence of coupled resonators where power is transfered into the fundamental mode in reflection. The transfer is only efficient if a high intensity field is present in the resonator as in resonance. The fundamental mode reflection is driven by the resonant field within the resonator via the out-of-band reflection. Simulations have shown that significant reflection occurs for an out-of-band intensity reflection factor as small as 10^{-4}.

The transmission of about 35% is accompanied in resonance by a narrow-band reflection of almost the same magnitude. The free spectral range FSR $= 270$ pm is measured with the coarse scanning mode of the tunable laser resulting in a finesse of $\mathcal{F} = 34$. For comparison an ordinary grating with a comparable reflection spectrum would require a length of about 180 mm. Considering the strength of the gratings the finesse is rather low.

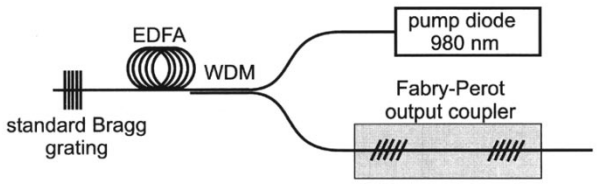

Fig. 9. Setup of a fiber laser with a mode-converting Bragg grating Fabry–Perot output coupler.

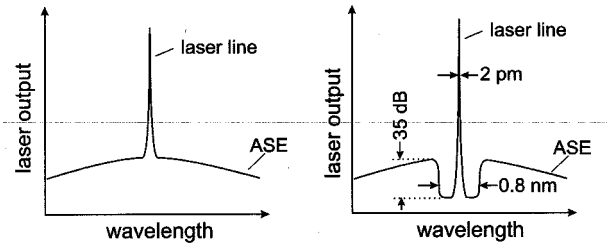

(a) (b)

Fig. 10. Comparison of a mode converting Bragg grating Fabry–Perot output coupler with a broad-band conventional output coupler.

This is caused in part by losses of the gratings and the two-mode section due to the UV writing process [6], [7]. In contrast to the case with "no reflection in resonance" here transmission and reflection occurs in the higher order mode as will be shown later. This light is lost in the adjacent single-mode fiber and adds to the insertion loss.

VI. Narrow-Band Output Coupler for Fiber Lasers

The mode-converting Fabry–Perot interferometer with narrow-band reflection in resonance is demonstrated as an output coupler for fiber lasers. The setup of a fiber laser with a mode-converting Fabry–Perot output coupler is shown in Fig. 9.

The advantage of this output coupler is illustrated in Fig. 10. If a broad-band mirror is used as an output coupler additionally to the light at the lasing wavelength also the broad-band ASE spectrum is leaving the cavity, thus degrading the laser output spectrum [see Fig. 10(a)]. This is true in particular for high-power lasers with a high-output coupling ratio.

In contrast an output coupler set up by a mode-converting Fabry–Perot interferometer exhibits on either side next to the resonance a strong return loss due to the mode-converting grating stop-band [see Fig. 10(b)]. Outside the grating stop-band a broad-band filter can be used to suppress the rest of the ASE noise floor. The return loss depends on the grating strength and can be made stronger than for example -35 dB as shown in [4] for strong mode converting gratings in two-mode fiber sections.

The output spectrum and the power characteristics of the fiber laser are displayed in Fig. 11.

The filter bandwidth is not narrow enough to allow operation of the laser on a single longitudinal mode.

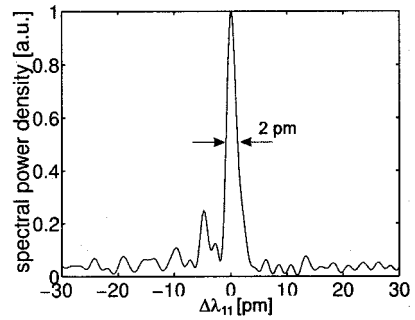

(a)

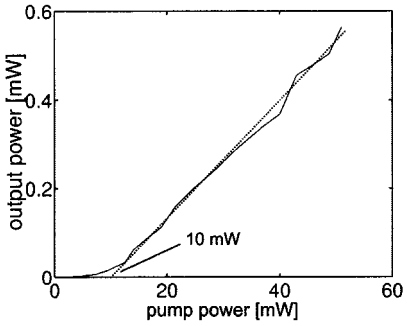

(b)

Fig. 11. Spectrum and power characteristics of the fiber laser with a Fabry–Perot interferometer setup with mode-converting gratings as the output coupler. (Length of the Erbium-doped fiber 6 m, Er^{3+}-concentration 600 ppm wt. Data of the standard Bragg grating: length 5 mm, FWHM bandwidth 0.6 nm and reflectivity 99%.)

VII. Tuning the Fabry–Perot Interferometer

Whether the mode-converting Fabry–Perot interferometer exhibits reflection in resonance or not is determined by the propagation constants β_{01} and β_{11} of the fundamental mode and the first higher order mode, respectively. This will be investigated with a mathematical model later in this paper in more detail.

By UV illumination of the fiber core in between the mode-converting gratings, as shown in Fig. 12, the core index increases. This causes the increase of the propagation constants of the LP_{01}- and LP_{11}-mode and according to the resonance condition (18) the Fabry–Perot interferometer undergoes consecutive resonances in transmission during exposure. The effective index of the fundamental mode increases faster than the effective index of the higher order mode due to the larger field overlap with the fiber core.

The measurement setup is similar to the one shown in Fig. 3. The narrow-band tunable laser source is set here to a fixed wavelength within the stop-band of the Fabry–Perot interferometer during the UV illumination. The setup allows to measure both the transmission and the reflection. The result of the experiment is displayed in Fig. 13 and shows that a narrow-band reflection only occurs in resonance of the Fabry–Perot interferometer. At the beginning of the UV illumination no reflection is recorded in resonance. With increasing exposure time a narrow-band reflection is present in resonance. After even longer exposure times the reflection vanishes again and then a new cycle starts.

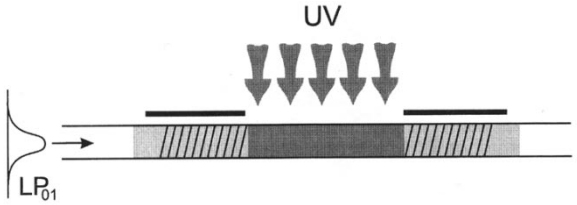

Fig. 12. Illumination of the fiber section between the mode-converting gratings.

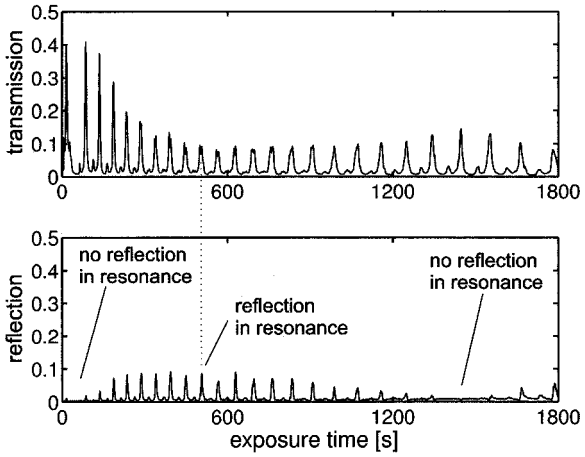

Fig. 13. Recording of the transmission and reflection factors during UV exposure of the fiber section between the mode-converting gratings of the Fabry–Perot interferometer.

Note that the overall decrease of total power with UV exposure time is due to UV-induced losses of various origins [6], [7]. Observations show that the losses due to absorption decrease in part with time after the exposure.

VIII. Mathematical Model

A mathematical model for the mode-converting Fabry–Perot interferometer is given by extending the standard Fabry–Perot formula by an extra term accounting for the effect of out-of-band reflection as indicated in Fig. 7.

Throughout this section index "0" ("1") stands for a property of the fundamental mode (first higher order mode). Double indexes stand for a transition between the modes denoted by the two indexes. The mathematical model assumes an equal and symmetric grating pair, e.g., no chirped gratings.

The propagation of the light between the mirrors is given in matrix notation by

$$\mathbf{P} = \begin{pmatrix} e^{-j\beta_0 L} & 0 \\ 0 & e^{-j\beta_1 L} \end{pmatrix} \tag{2}$$

where L is the grating separation. Similarly, the amplitude reflection and conversion coefficients are comprised within matrix $\mathbf{R}$ and accordingly for transmission by matrix $\mathbf{T}$:

$$\mathbf{R} = \begin{pmatrix} r_{00} & c_{01} \\ c_{01} & r_{11} \end{pmatrix}, \quad \mathbf{T} = \begin{pmatrix} t_{00} & 0 \\ 0 & t_{11} \end{pmatrix} \tag{3}$$

Matrix $\mathbf{A}$ is defined as:

$$\mathbf{A} = \mathbf{PR} = \begin{pmatrix} r_{00}e^{-j\beta_0 L} & c_{01}e^{-j\beta_0 L} \\ c_{01}e^{-j\beta_1 L} & r_{11}e^{-j\beta_1 L} \end{pmatrix}, \quad a_{kl} = (\mathbf{A})_{kl}. \tag{4}$$

Starting with an incident wave with the amplitude E_i of the electric field the multiple beam interference in transmission results in an infinite sum:

$$\begin{pmatrix} E_{t0} \\ E_{t1} \end{pmatrix} = \mathbf{T}\sum_{N=0}^{\infty}\mathbf{A}^{2N}\mathbf{PT}\begin{pmatrix} E_i \\ 0 \end{pmatrix} = \frac{t_{00}E_i e^{-j\beta_0 L}}{(1+|\mathbf{A}|)^2-(tr\cdot\mathbf{A})^2} \times \begin{pmatrix} t_{00}\left(1-a_{22}^2-a_{12}a_{21}\right) \\ t_{11}a_{21}(a_{11}+a_{22}) \end{pmatrix}. \tag{5}$$

Where the relation

$$\sum_{N=0}^{\infty}\mathbf{A}^{2N} = \frac{\begin{pmatrix} 1-a_{22}^2-a_{12}a_{21} & a_{12}(a_{11}+a_{22}) \\ a_{21}(a_{11}+a_{22}) & 1-a_{11}^2-a_{12}a_{21} \end{pmatrix}}{(1+|\mathbf{A}|)^2-(tr\cdot\mathbf{A})^2} \tag{6}$$

has been used. Equation (6) can be derived by diagonalizing $\mathbf{A}$ and evaluating the infinite sum similar to the well-known text book Fabry–Perot interferometer derivation.

Similarly, the reflected electrical field is written as

$$\begin{pmatrix} E_{r0} \\ E_{r1} \end{pmatrix} = \mathbf{R}\begin{pmatrix} E_i \\ 0 \end{pmatrix} + \mathbf{TA}\sum_{N=0}^{\infty}\mathbf{A}^{2N}\mathbf{PT}\begin{pmatrix} E_i \\ 0 \end{pmatrix}. \tag{7}$$

With the infinite sum evaluated (7) takes the form

$$\begin{pmatrix} E_{r0} \\ E_{r1} \end{pmatrix} = \mathbf{R}\begin{pmatrix} E_i \\ 0 \end{pmatrix} + \frac{t_{00}E_i e^{-j\beta_0 L}}{(1+|\mathbf{A}|)^2-(tr\cdot(\mathbf{A})^2} \times \begin{pmatrix} t_{00}\left(a_{11}\left(1-a_{22}^2\right)+a_{12}a_{21}a_{22}\right) \\ t_{11}a_{21}(1+a_{11}a_{22}-a_{12}a_{21}) \end{pmatrix}. \tag{8}$$

The exact solution for the mode-converting Fabry–Perot interferometer with out-of-band reflection under the assumptions made above is given by (5) and (7). The normalized spectral intensity transmission and reflection factor is calculated by multiplying the according electric field by its complex conjugate.

The condition for the occurrence of fundamental mode reflection in resonance as recorded experimentally in Fig. 8 is of practical interest for a well defined fabrication of, e.g., either nonreflecting transmission filters or output couplers. For this purpose an approximation for the normalized spectral intensity transmission and reflection factor is derived up to terms linear in R

$$\begin{aligned}
\frac{I_{t_0}}{I_0} &\approx \frac{T^2\{1+C^2-2C\cos[(\beta_0+\beta_1)L-2\phi_c]+Rg_1\}}{\{1+C^2-2C\cos[(\beta_0+\beta_1)L-2\phi_c]\}^2+Rg_2} \\
g_1 &= 2C\cos[(\beta_0-\beta_1)L-2\phi_c+2\phi_{r_{11}}] \\
&\quad -2\cos(2\beta_1 L-2\phi_{r_{11}}) \\
g_2 &= 4C\cos[(\beta_1-\beta_0)L-2\phi_c+2\phi_{r_{00}}] \\
&\quad +4C\cos[(\beta_0-\beta_1)L-2\phi_c+2\phi_{r_{11}}] \\
&\quad +8C^2\cos[(\beta_0+\beta_1)L-\phi_{r_{00}}-\phi_{r_{11}}] \\
&\quad -2\cos(2\beta_0 L-2\phi_{r_{00}})-2\cos(2\beta_1 L-2\phi_{r_{11}}) \\
&\quad -4C\cos[2(\beta_0+\beta_1)L+2\phi_c+\phi_{r_{00}}+\phi_{r_{11}}] \\
&\quad -2C^2\cos(2\beta_1 L-4\phi_c-2\phi_{r_{00}}) \\
&\quad -2C^2\cos(2\beta_0 L-4\phi_c+2\phi_{r_{11}}) \\
&\quad -4C^3\cos(\phi_{r_{00}}+\phi_{r_{11}}-2\phi_c).
\end{aligned} \tag{9}$$

Here, $\phi_s = \arg(s)$, where s stands for $c_{01}, r_{00}, r_{11}, t_{00}$ or t_{11}, respectively

$$\begin{aligned}
\frac{I_{r_0}}{I_0} &\approx R + R \\
&\quad \times \frac{Tg_3+T^2g_4}{\{1+C^2-2C\cos[(\beta_0+\beta_1)L-2\phi_c]\}^2+Rg_2} \\
g_3 &= 2\cos(2\beta_0 L-2\phi_{t_{00}}) \\
&\quad -4C\cos[(\beta_0-\beta_1)L+2\phi_c-2\phi_{t_{00}}] \\
&\quad +2C^2\cos(2\beta_1 L-4\phi_c+2\phi_{t_{00}}) \\
&\quad +2C\cos[2(\beta_0+\beta_1)L+\phi_{r_{00}}-\phi_{r_{11}}-2\phi_c-2\phi_{t_{00}}] \\
&\quad -4C^2\cos[(\beta_0+\beta_1)L+\phi_{r_{00}}-\phi_{r_{11}}-2\phi_{t_{00}}] \\
&\quad +2C^3\cos(\phi_{r_{00}}-\phi_{r_{11}}+2\phi_c-2\phi_{t_{00}}) \\
g_4 &= 1+C^2+2C\cos(2\beta_1 L+\phi_{r_{00}}-\phi_{r_{11}}-2\phi_c).
\end{aligned} \tag{10}$$

The above approximate expressions are further simplified by assuming explicit values for the amplitude reflection and transmission factors for Bragg gratings under LP_{01}-LP_{11} phase matching condition. With the assumption of power conservation and zero cross transmission $t_{01} = t_{10} = 0$ (zero off-diagonal elements in Matrix $\mathbf{T}$), the following relations can be derived from multiport theory:

$$c_{01} = -\sqrt{C} \Rightarrow \phi_c = \pi \tag{11}$$

$$r_{00} = -j\sqrt{R} \Rightarrow \phi_{r_{00}} = -\frac{\pi}{2} \tag{12}$$

$$r_{11} = r_{00} \Rightarrow \phi_{r_{11}} = -\frac{\pi}{2} \tag{13}$$

$$t_{00} = \sqrt{T} \Rightarrow \phi_{t_{00}} = 0, \quad \text{where } T = 1-C-R \tag{14}$$

$$t_{11} = -\sqrt{T} \Rightarrow \phi_{t_{11}} = \pi \tag{15}$$

Equations (9) and (10) yield with (11)–(15):

$$\begin{aligned}
\frac{I_{t_0}}{I_0} &\approx T^2\frac{1+C^2-2C\cos[(\beta_0+\beta_1)L]+Rh_1}{\{1+C^2-2C\cos[(\beta_0+\beta_1)L]\}^2+Rh_2} \\
h_1 &= 2\cos(2\beta_1 L)-2C\cos[(\beta_0-\beta_1)L] \\
h_2 &= 4C^3+(2+2C^2)(\cos(2\beta_0 L)+\cos(2\beta_1 L)) \\
&\quad +4C\cos[2(\beta_0+\beta_1)L] \\
&\quad -8C^2\cos[(\beta_0+\beta_1)L]-8C\cos[(\beta_0-\beta_1)L]
\end{aligned} \tag{16}$$

$$\begin{aligned}
\frac{I_{r_0}}{I_0} &\approx R + R\frac{Th_3+T^2h_4}{\{1+C^2-2C\cos[(\beta_0+\beta_1)L]\}^2+Rh_2} \\
h_3 &= 2\cos(2\beta_0 L)-4C\cos[(\beta_0-\beta_1)L]+2C^2\cos(2\beta_1 L) \\
&\quad +2C\cos[2(\beta_0+\beta_1)L]-4C^2\cos[(\beta_0+\beta_1)L] \\
&\quad +2C^3 \\
h_4 &= 1+C^2+2C\cos(2\beta_1 L)
\end{aligned} \tag{17}$$

The resonance condition of the Fabry–Perot interferometer is given by finding the minimum of the denominator in (16). If the term Rh_2 is neglected the resonance condition is given by

$$\cos[(\beta_0+\beta_1)L] = 1. \tag{18}$$

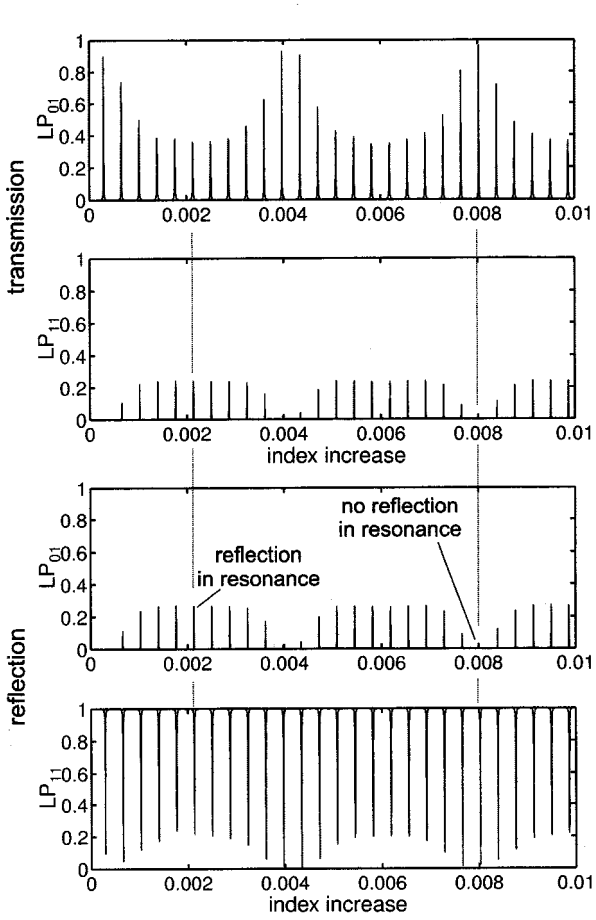

Fig. 14. Calculation of the intensity transmission and reflection factors of the LP_{01} and LP_{11}-mode versus the UV-induced index increase comparable to the experiment outlined in Fig. 12.

The comparison of (16) and (17) indicates that the reflection in resonance is much narrower compared to the transmission (see Fig. 8) because neglecting R in (16) allows to cancel the numerator. In reflection [see (17)] that is not possible and the denominator is still squared. It can be shown that the numerator here varies only slowly across a resonance. Hence, the resonance in reflection is narrower than the resonance in transmission.

Equation (17) further shows that out of resonance a fundamental mode reflection of size R is present. This reflection is independent whether narrow band reflection occurs in resonance or not. That means a nonreflecting filter can only be set up by pure mode-converting mirrors. However, the out-of-band reflection for the Bragg gratings discussed here are well below $R = 10^{-3}$ giving a return loss in excess of -30 dB. With the use of (5) and (7) the intensity transmission and reflection factors of the fundamental mode and first higher order mode versus the UV-induced index increase comparable to the experimental results shown in Fig. 13 are calculated. The results are displayed in Fig. 14 and are in good agreement with the experimental observation. Please note that the reflection and transmission of the first higher order mode were not recorded in the experiment because they are not guided by the adjacent single mode fiber and cannot be detected with the setup described above. The index increase of the core is sensed by the two propagating modes differently. This leads to a differential change of the propagation constants β_0 and β_1. The small contribution of the out-of-band reflection, that is producing the fundamental mode reflection in resonance, also results in a LP_{11}-mode transmission (see Fig. 14). Regarding the output coupler, this light is lost and causing extra loss of the component.

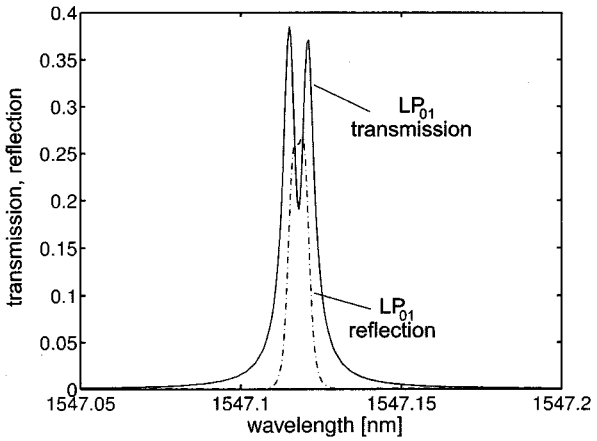

Fig. 15. Calculation of the fundamental mode intensity transmission and reflection factor at a resonance of the mode-converting Fabry–Perot interferometer.

Fig. 15 shows the calculation of the intensity transmission and reflection factor of one individual Fabry–Perot resonance and is in good agreement with the experimental results of Fig. 8. This calculation further shows, as mentioned before, that the resonance in reflection is significantly narrower than the resonance in transmission. Even the splitting of the transmission resonance (see Fig. 8) is produced by the model calculation. In order to derive the condition for fundamental mode reflection in resonance we start with the resonance condition according to (18). The propagation constants satisfy in resonance

$$e^{-j\beta_0 L} = (e^{-j\beta_1 L})^* \Rightarrow \mathbf{A} = \begin{pmatrix} -j\sqrt{R}(e^{-j\beta_1 L})^* & -\sqrt{C}(e^{-j\beta_1 L})^* \\ -\sqrt{C}e^{-j\beta_1 L} & -j\sqrt{R}e^{-j\beta_1 L} \end{pmatrix}. \quad (19)$$

The normalized spectral intensity transmission and reflection factors for resonance [see (18)] are calculated from (5) and (8) with (11)-(15)

$$\left.\frac{I_{t_0}}{I_0}\right|_{\text{res}} = T^2\frac{(1-C)^2 + R^2 + 2R(1-C)\cos(2\beta_1 L)}{HN}$$

$$HN = T^4 + 6R^2 + 4T^2R + 2R^2\cos(4\beta_1 L) + (8R^2 + 4T^2R)\cos(2\beta_1 L) \quad (20)$$

$$\left.\frac{I_{r_0}}{I_0}\right|_{\text{res}} = R + \{2RT[R + (C+R)(T^2+2R) + (T^2 + 2R + 2RC + 2R^2)\cos(2\beta_1 L)] + 2RT[R\cos(4\beta_1 L)] + RT^2[1 + C^2 + 2CR + R^2 + 2(R+C)\cos(2\beta_1 L)]\}/HN. \quad (21)$$

According to (21) with the Fabry–Perot interferometer in resonance $\cos(2\beta_1 L) \neq -1$ is necessary for narrow-band funda-

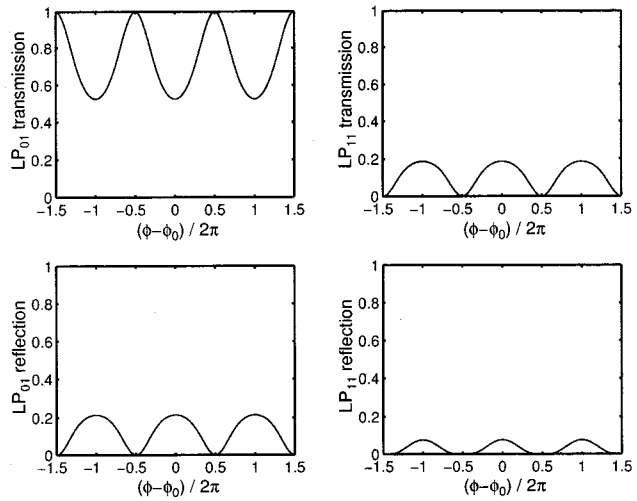

Fig. 16. Intensity transmission and reflection factors of a mode-converting Fabry–Perot interferometer in resonance ($C = 0.9$ and $R = 0.001$) for $(\beta_0 + \beta_1)L = 2\pi n, n \in \mathbf{N}$.

mental mode reflection. A maximum in reflection is reached for $\cos(2\beta_1 L) = 1$. By using the resonance condition of (18) this can be rewritten as

$$\cos[(\beta_0 - \beta_1)L] = 1. \tag{22}$$

This is the condition for a maximum of fundamental mode reflection in resonance. In order to show that this result is in agreement with the experimental result of Fig. 13 and the calculation of Fig. 14 we evaluate (20) and (21) (see Fig. 16), where $\phi = (\beta_0 - \beta_1)L$ is the argument of (22). ϕ_0 denotes a phase for which the fundamental mode reflection has a maximum. In Fig. 16 we further calculated the transmission and reflection of the higher order mode in resonance. For a fixed wavelength λ the phase ϕ is only depending on the change of the difference of the effective index during UV exposure. Fig. 16 has then to be interpreted as the envelope of the experimental result of Fig. 13 and the calculation of Fig. 14, respectively.

Fig. 16 undergoes consecutive periods and in turn the mode of operation of the Fabry–Perot interferometer changes periodically from "no reflection in resonance" to "reflection in resonance." It is therefore possible to design the mode-converting Fabry–Perot interferometer either with or without reflection in resonance, e.g., by tuning the core index of the fiber by UV illumination as shown experimentally in Fig. 13.

IX. Conclusion

We have presented a mode-converting Fabry–Perot interferometer fabricated with tilted Bragg gratings in a two-mode section of an elsewhere single-mode fiber. We demonstrated this interferometer as a nonreflecting narrow-band transmission filter. In the presence of out-of-band reflection, we have analyzed the condition for simultaneous narrow-band reflection and transmission in resonance. This effect was applied to fabricate a narrow-band output coupler for a fiber laser. A mathematical model has been given showing that a coupled resonance is responsible for the observed reflection. We have demonstrated that the Fabry–Perot interferometer can be fabricated in either mode of operation by UV tuning of the resonator.

Acknowledgment

The authors would like to acknowledge the OFTC Sydney for supplying the photosensitive fiber (CD 120.02) used in these experiments.

References

[1] T. A. Strasser, J. R. Pedrazzani, and M. J. Andrejco, "Reflective-mode conversion with UV-induced phase gratings in two-mode fiber," presented at the Conference on Optical Fiber Communication, OSA Technical Digest Series, vol. 6, Washington, D.C., 1997. paper FB3.

[2] C. K. Madsen, T. A. Strasser, M. A. Milbrodt, C. H. Henry, A. J. Bruce, and J. J. DeMarco, "Planar waveguide add/drop filter employing a mode-converting grating in an adiabatic coupler," in *Proc. Integrated Photonics Research Conf.*, Victoria, BC, Canada, 1998, pp. 102–104. IMG5.

[3] D. Johlen, H. Renner, A. Ewald, and E. Brinkmeyer, "Fiber Bragg grating Fabry-Perot interferometer for a precise measurement of the UV-induced index change," in *Proc. ECOC'98*, Madrid, Spain, 1998, Paper WdA06, pp. 393–394.

[4] D. Johlen, H. Renner, P. Klose, and E. Brinkmeyer, "UV-writing of two-mode sections into single-mode fibers for hosting mode-converting Bragg gratings," *IEEE Photon. Technol. Lett.*, vol. 11, pp. 1015–1017, 1999.

[5] D. Johlen, P. Klose, A. Ewald, and E. Brinkmeyer, "Non-reflecting narrow-band fiber optical Fabry-Perot transmission filter," in *Proc. Bragg Gratings, Photosensitivity and Poling in Glass Fibers and Waveguides: Applications and Fundamentals Meeting*. Williamsburg, VA, 1997, Paper BSuC5, pp. 42–44.

[6] D. Johlen, F. Knappe, H. Renner, and E. Brinkmeyer, "UV-induced absorption, scattering and transition losses in UV side-written fibers," in *Proc. Conf. Optical Fiber Communication, OSA Tech. Dig. Series*. Washington, D.C., 1999, Paper ThD1.

[7] H. Renner, D. Johlen, and E. Brinkmeyer, "Modal field deformation and transition losses in UV-side written optical fibers," *Appl. Opt.*, vol. 39, no. 6, Feb. 2000.

[8] D. Johlen, P. Klose, H. Renner, and E. Brinkmeyer, "Strong LP_{11}-mode splitting in UV side-written tilted fiber gratings," in *Bragg Gratings, Photosensitivity and Poling in Glass Fibers and Waveguides: Applications and Fundamentals Meeting*. Williamsburg, VA, 1997, Poster BMG12, pp. 219–221.

[9] ——, "Narrow-band mode-converting Fabry-Perot output coupler for fiber lasers," in *Proc. Conf. Optical Fiber Communication, OSA Tech. Dig. Series*, vol. 2. Washington, D.C., 1998, Paper FA4, pp. 372–373.

Dietmar Johlen, photograph and biography not available at the time of publication.

Peter Klose, photograph and biography not available at the time of publication.

Hagen Renner, photograph and biography not available at the time of publication.

Ernst Brinkmeyer, photograph and biography not available at the time of publication.